A computational model for capturing the distinct in- and out-of-plane response of lipid membranes

Pinjing Wen[1,2,3], Xi Wei[3], and Yuan Lin [*3]

[1]Institute of Semiconductor Manufacturing Research, Shenzhen University, Shenzhen, 518060, Guangdong, China
[2]College of Physics and Optoelectronic Engineering, Shenzhen University, Shenzhen 518060, Guangdong, China
[3]Department of Mechanical Engineering, The University of Hong Kong, Hong Kong SAR, China.

October 4, 2020

1 Abstract

A computational framework was developed to capture the combined fluid- and solid-like behavior of lipid membranes in a unified manner. Specifically, the in-plane diffusion of lipid molecules and the associated evolution of membrane tension were explicitly taken into account in the model. In addition, the out-of-plane movement induced bending and shearing of membrane, along with its thermal undulations caused by bombardment of medium molecules, were also considered. The capability and validity of this approach were demonstrated by simulating the enforced deformation and shape fluctuations of a lipid vesicle under a variety of testing conditions as well as their comparison with corresponding theoretical predictions. Our model could serve a useful platform for investigating processes such as cell spreading and division where morphology evolution of the membrane and transport of lipids/transmembrane proteins are known to play key roles.

2 Introduction

Cell membrane is a phospholipid bilayer, with a thickness of only a few nanometer, embedded with various proteins [1]. Physically, the interactions among

*Corresponding author: ylin@hku.hk

phospholipids and their mobility give both elasticity and fluidity to the membrane as well as restrict lateral diffusion of transmembrane proteins [2]. It is well known that besides serving as a physical barrier, cell membrane also plays a key role in many important cellular processes such as cell spreading, adhesion, division etc [3, 4]. For this reason, intense effort has been invested over the past few decades to understand and model the mechanical behavior of cell membrane. For example, the membrane was often treated as an elastic layer or a network consisting of different biological molecules with small or infinitesimal thickness. Following classical theory of elastic thin-shells, the response of membrane against bending was considered by many researchers [5, 6, 7]. In addition, by adopting fluid-like elastic constitutive laws with volume and area constraints, different finite element models have also been proposed to study lipid membrane deformation [8, 9, 10, 11].

It must be pointed out that, these continuum mechanics-based formulations did not consider the distinct roles of different constituents within the membrane. This issue was first addressed by the so-called mosaic model [12] where the membrane was treated as a two dimensional liquid with different embedded molecules. Following such picture, Saffman et al. [13, 14] examined the lateral and rotational Brownian diffusion of transmembrane proteins (simplified as cylinders embedded in the lipid-bilayer). In addition, the mechanisms by which specialized proteins capable of inducing shape remodeling of the membrane [15, 16] and eventually directing certain cellular functions [17, 18] have been extensively investigated.

Despite these aforementioned efforts, several important things remain unsettled. First of all, it is well-known that, microscopically, the mechanical response of phospholipid bilayer originates from the hydrophobic/hydrophilic nature of the lipid molecule [19, 20]. Specifically, within the membrane, hydrophilic heads of lipids are exposed to water while the hydrophobic tails are hided in the middle of the bi-layer (refer to Figure 1). The lipid molecule can freely move within each layer by lateral diffusion, leading to the fluid-like in-plane behavior of the membrane. A reduced lipid density in certain region will expose the hydrophobic tails to water and result in an elevated in-plane tension locally [21], as well as cause lipids nearby to "flow" into this region [22] and make the tension within the membrane more homogeneous. However,to the best of our knowledge, such coupling lipid transport with membrane tension in membrane deformation has not been established in existing models. In addition, the bi-layer structure will be under constant bombardment of medium molecule, resulting in spontaneous undulations of the membrane [23, 24]. But, a method allowing us to introduce such thermal excitation to membrane in a seamless manner is still lacking.

Aiming to address these outstanding problems, we proposed a new computational model where lipid molecules were allowed to diffuse within the membrane despite being constrained by internal forces including in-plane tension and bending moment. In addition, a random (both spatially and temporally) force distribution on the membrane was also introduced to represent thermal undulations. The validity and capability of the method were demonstrated through several numerical examples as well as comparison with theoretical predictions.

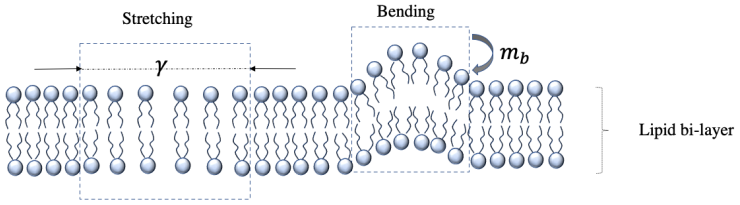

Figure 1: Schematic plot of a deformed lipid bi-layer membrane

3 Formulation

The linear diffusion equation, characterizing the collective motion of micro-particles in a material resulting from their individual random movement, can be used to describe the transport of lipid molecules within the membrane as

$$\frac{\partial \rho}{\partial t} = D\nabla^2 \rho \tag{1}$$

where ρ and D are the areal density and diffusivity of lipid molecules. Since the resistance of membrane against expansion originates from the extra hydrophobic area exposed to water upon stretching, a nonuniform density distribution of lipid molecules will lead to a non-homogeneous surface tension within the membrane. Such effect can be taken into account as

$$\gamma = -K_A(\frac{\rho - \rho_0}{\rho_0}) \tag{2}$$

where K_A is the so-called area expansion modulus [25] and ρ_0 represents the reference lipid density (i.e. the density leading to zero membrane tension). Note that, during bending deformation, one layer of lipids is stretched while the other undergoes compression (refer to Fig. 1), both leading to an elevated energy of membrane. This means that the bi-layer membrane also possesses a bending stiffness κ_b (against out-of-plane deformations). According to the shell theory, the bending moment developed within the membrane can be expressed as

$$m_b = \kappa_b(C_1 + C_2) \tag{3}$$

where C_1 and C_2 are the two principal curvatures of the deformed membrane.

Next, to capture the shape evolution of the cell/vesicle membrane (immersed in a viscous fluid), the immersed boundary integral method was adopted where the velocity of membrane at point ξ can be evaluated by [26, 27].

$$u_i(\xi) = \int\int_S u_i^j(\xi, \mathbf{y}) n_j(\mathbf{y}) \Delta\sigma(\mathbf{y}) \mathrm{d}S_{\mathbf{y}} \tag{4}$$

where

$$u_i^j(\xi, \mathbf{y}) = -\frac{1}{8\pi\mu}\left(\frac{\delta_{ij}}{r} + \frac{(\xi_i - y_i)(\xi_j - y_j)}{r^3}\right), \tag{5}$$

is the fundamental solution of the Stokes equation with $r = |\xi - \mathbf{y}|$, located at point $\mathbf{y}$ and oriented in the j^{th} direction. Here $\mathbf{n}$ represents the unit out-normal vector of membrane, and μ is the cytosol viscosity.

The term $\Delta\sigma$ contains contributions from the tension-induced pressure difference across the membrane as well as the transverse shear stress (in the normal direction) developed within the bi-layer. From Young-Laplace law, the pressure difference σ_p can be found as

$$\sigma_p = \gamma(C_1 + C_2) \tag{6}$$

On the other hand, according to the elastic shell theory, the transverse shear stress within membrane is related to the bending moment as

$$\sigma_s = \nabla^2 m_b \tag{7}$$

where ∇^2 stands for the Laplace operator. Therefore, $\Delta\sigma$ can be found to take the form

$$\Delta\sigma = \sigma_s + \sigma_p = \nabla^2 m_b + \gamma(C_1 + C_2). \tag{8}$$

To avoid the singularity presented in Eq. (4) (as $\mathbf{y}$ approaches ξ), we can re-write it as [28]

$$u_i(\xi) = \int\int_S u_i^j(\xi, \mathbf{y}) n_j(\mathbf{y})[\Delta\sigma(\mathbf{y}) - \Delta\sigma(\xi)]\mathrm{d}S_{\mathbf{y}} + \Delta\sigma(\xi)\int\int_S u_i^j(\xi, \mathbf{y}) n_j(\mathbf{y})\Delta\sigma(\mathbf{y})\mathrm{d}S_{\mathbf{y}} \tag{9}$$

where the first term on the right hand side is a regular integral while the second term vanishes for any self-enclosed membrane. In the end, we have

$$u_i(\xi) = \int\int_S u_i^j(\xi, \mathbf{y}) n_j(\mathbf{y})[\Delta\sigma(\mathbf{y}) - \Delta\sigma(\xi)]\mathrm{d}S_{\mathbf{y}}, \tag{10}$$

an expression that is readily to be used in simulating the shape evolution of membrane.

4 Implementation in FEM simulations

The finite element method was used to calculate the in-plane tension (or equivalently the lipid density distribution), transverse shear and bending moment developed in the membrane. Specifically, the membrane was meshed by a network of three-node triangles. According to Eq. (1), lipid density evolution at point $\mathbf{x_i}$ in the membrane can be captured by

$$\frac{\rho(\mathbf{x_i}, t+\Delta t) - \rho(\mathbf{x_i}, t)}{\Delta t} = D\frac{\int_{A(\mathbf{x_i})} \Delta\rho(\mathbf{x_i}, t) dA(\mathbf{x_i})}{A(\mathbf{x_i})} \tag{11}$$

where t corresponds to time, $A(\mathbf{x_i})$ is the area/domain surrounding nodal point $\mathbf{x_i}$(refer to Fig.2). By applying the discrete form of the Laplace-Beltrami equation (see Appendix A for details), Eq. (11) can be re-written as

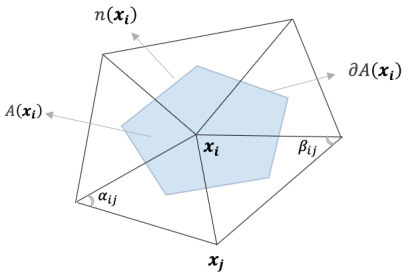

Figure 2: Definition of the area $A(\mathbf{x_i})$, as well as its boundary $\partial A(\mathbf{x_i})$, surrounding a nodal point $\mathbf{x_i}$ in our numerical scheme. Note that, each side of $\partial A(\mathbf{x_i})$ crosses the mid-point of the segment $\mathbf{x_i x_j}$, connecting $\mathbf{x_i}$ and a neighboring point $\mathbf{x_j}$.

$$\frac{\rho(\mathbf{x_i}, t+\Delta t) - \rho(\mathbf{x_i}, t)}{\Delta t} = D\frac{\sum_j (\cot\alpha_{ij} + \cot\beta_{ij})(\rho(\mathbf{x_j}, t) - \rho(\mathbf{x_i}, t))}{2A(\mathbf{x_i})} \tag{12}$$

where $\mathbf{x_j}$ represents a neighboring nodal point of $\mathbf{x_i}$ while α_{ij} and β_{ij} correspond to the two opposite angles of edge $\mathbf{x_i x_j}$ (refer to Fig.2). Once ρ is known, the in-plane tension γ of membrane can then be calculated and updated from Eq. (2).

Next, notice that the mean curvature H_i (defined as the average of two principle curvatures, i.e. $H_i = (C_1 + C_2)/2$) at a triangle element node $\mathbf{x_i}$ can be evaluated as [29, 30]

$$\Delta\mathbf{x_i} = -2\ H_i\mathbf{n} \tag{13}$$

where $\mathbf{n}$ is the unit normal vector of the deformed surface at position $\mathbf{x_i}$. Therefore, σ_p at point $\mathbf{x_i}$ can be expressed as

$$\sigma_p(\mathbf{x_i}) = 2\gamma H_i = \gamma \frac{\sum_j (\cot\alpha_{ij} + \cot\beta_{ij})(\mathbf{x_j} - \mathbf{x_i})}{A(\mathbf{x_i})} \tag{14}$$

The bending moment within the membrane is simply

$$m_b(\mathbf{x_i}) = 2\kappa_b H_i \tag{15}$$

from which the transverse shear stress can be found as

$$\sigma_s(\mathbf{x_i}) = \frac{\sum_j (\cot\alpha_{ij} + \cot\beta_{ij})(m_b(\mathbf{x_j}) - m_b(\mathbf{x_i}))}{2A(\mathbf{x_i})}. \tag{16}$$

Finally, from the boundary integral expression (i.e. Eq. (10)), the moving velocity of membrane can be determined by

$$u_j(\mathbf{x_i}) = -\frac{1}{8\pi\mu} \sum_{m=1}^{M} (\Delta\sigma_j(\mathbf{x_m}) - \Delta\sigma_j(\mathbf{x_i}))[\sum_{k=1}^{3} \left(\frac{\delta_{kj}}{r} + \frac{(\mathbf{x_i}_j - \mathbf{x_m}_j)(\mathbf{x_i}_k - \mathbf{x_m}_k)}{r^3} \right) A(\mathbf{x_m})\mathbf{n}_k(\mathbf{x_m})] \tag{17}$$

where j and k mean the j^{th} and k^{th} components of a vector while M represents the total number of nodes over the membrane. Once the velocity field is known, the shape evolution of the cell/vesicle can then be determined by simple temporal integration.

5 Result and discussion

The computational model described above was then used to simulate the response of a membrane vesicle (with an initial radius of $R = 1\mu m$ and immersed in the cytosol with viscosity $\mu = 1.2Pa \cdot s$ [31]) under various experimental conditions. Note that, for lipid membrane, the diffusivity of lipid molecules is believed to be around $D = 1\mu m^2/s$ [31], the areal expansion modulus is of the order of $K_A = 1pN \cdot \mu m^{-1}$ while the bending rigidity is typically around $\kappa_b = 20k_BT$[32, 33] (with k_BT being the thermal energy). Therefore, the dimensionless areal expansion modulus $\tilde{K}_A = K_A R^2/\kappa_b$ should be of the order of 10. We then non-dimensionlized the problem by normalizing every length, force, and time variables with R, κ_b/R^2 and $\mu R^3/\kappa_b$ respectively. During the simulation, the vesicle surface was meshed by 1806 triangle elements defined by 3608 nodal points.We must point out that, since the deformation was relatively small in all the numerical examples presented here, no remeshing of the membrane surface was carried out in our FEM simulations. However, such step may become necessary once the distortion of membrane becomes severe.

5.1 In-plane transport of lipids

We first examined the evolution of lipid density (or equivalently the in-plane tension) distribution over the membrane when some lipid molecules were suddenly removed at the south pole of the vesicle. In this case, the initial membrane tension was taken to be zero (i.e. choosing $\rho = \rho_0$ at $t = 0$), and then a step decrease in the lipid density at the south pole of vesicle was introduced. According to Eq. (2), the sudden removal of lipids at the pole will result in a step increase in the membrane tension locally. On the other hand, such spatial variation in tension will decay gradually with respect to time as diffusion of lipid molecules makes their distribution more homogeneous. Indeed, as illustrated by Fig. 3 and 4, both the lipid density and tension distributions become more and more uniform, before eventually reaching a steady state. Of course, the diffusivity of lipids (D) and size of vesicle (R) largely determine how fast such homogeneous/steady-state configuration can be reached.

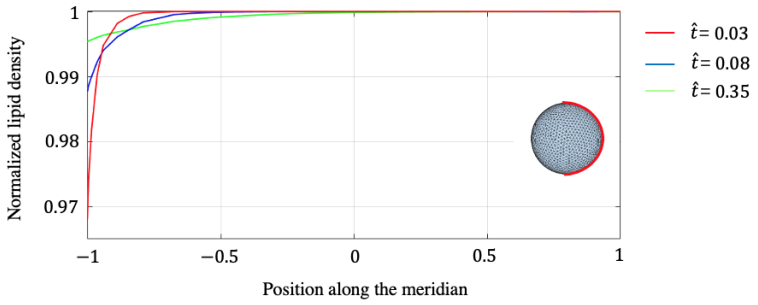

Figure 3: Lipid density ($\frac{\rho}{\rho_0}$) distribution along the meridian of the vesicle at three normalized time $\hat{t}$ points (i.e. $\hat{t} = \frac{t}{\mu R^3/\kappa_b} = 0.03, 0.08$ and 0.35). Here -1 and 1 on the horizontal axis correspond to the south and north pole of the vesicle, respectively.

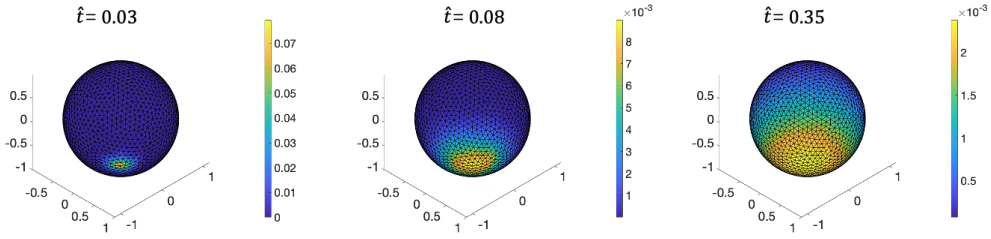

Figure 4: Snap-shots of the distribution of in-plane tension over the membrane ($\hat{t} = \frac{t}{\mu R^3/\kappa_b} = 0.03, 0.08$ and 0.35)

5.2 Shape evolution of vesicle under two stretching forces at two opposing poles

Next, we considered the coupling between the out-of-plane deformation of membrane with its in-plane tension evolution. In this case, two Gaussianly distributed pressures (i.e. $\sigma_t(\mathbf{x}) = p_0 * e^{-\frac{|\mathbf{x}-\mathbf{x_p}|^2}{2\pi(0.1)^2}}$, with $p_0 = 2Pa$ and $\mathbf{x_p} = (0, 0, -1)$ or $(0, 0, 1)$ for the south or north pole, respectively) were applied suddenly to opposing poles of the vesicle, that is this σ_t was added to Eq. (8) in the calculation.

Snap-shots of the deformed vesicle are shown in Fig. 5, where the configuration at $\hat{t} = 7$ essentially shows the steady-state/equilibrium shape of the vesicle. Interestingly, as both poles of the vesicle were pulled out, the membrane in those regions underwent stretching which led to a reduced lipid density as well as an elevated in-plane tension (Fig. 6). Such local changes in the density of lipids will then induce their transport within the membrane, effectively transmitting the influence of the applied loads to the other parts of the membrane.

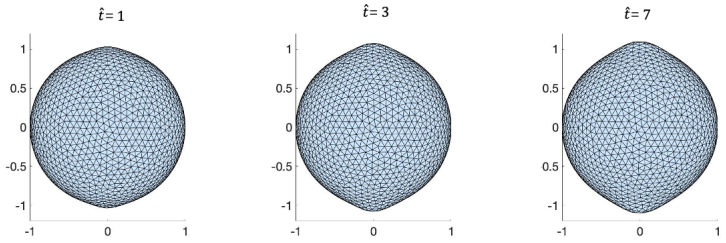

Figure 5: Snap-shots of vesicle shape evolution ($\hat{t} = \frac{t}{\mu R^3/\kappa_b} = 1, 3$ and 7)

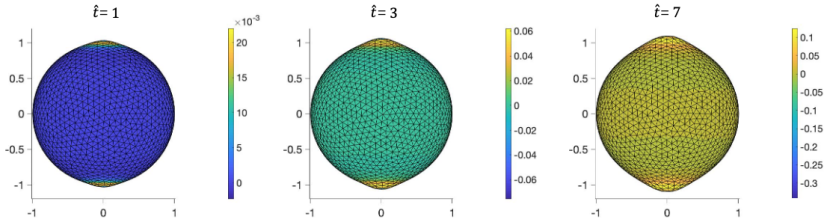

Figure 6: Snap-shots of in-plane tension distribution evolution over the membrane ($\hat{t} = \frac{t}{\mu R^3/\kappa_b} = 1, 3$ and 7)

5.3 Shape fluctuations of the vesicle

The nanometer range thickness of cell membrane makes it extremely susceptible to thermal induced bending deformations, which are actually visible under a microscope [34, 35]. Physically, this kind of thermal excitation originates from collisions between the membrane and surrounding medium molecules, as illustrated in Fig. 7(a).

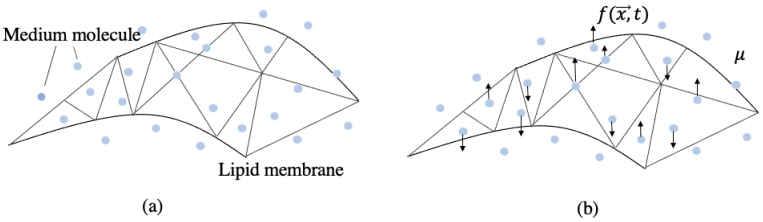

Figure 7: (a) Schematic of a lipid membrane immersed in the medium. (b)The effect of collisions of fluid molecules on the membrane can be represented by a randomly distributed load f.

To take such entropic effect into account in our model, a random force distribution f (along the normal direction of membrane) was introduced to represent continuous bombardments of fluid molecules on the membrane, a strategy similar to that for the case of bio-filaments [36, 37]. To be self consistent, this random force must be Gaussian with zero mean and relate to the bulk medium viscosity μ as

$$< f(\mathbf{x_i}, t) f(\mathbf{x_j}, \tau) >= 2\mu k_B T \delta(\mathbf{x_i} - \mathbf{x_j}) \delta(t - \tau) \tag{18}$$

where t and τ represent time, δ is the Dirac delta function, $\mathbf{x_i}$ and $\mathbf{x_j}$ are the position vectors and the brackets stand for average. Notice that, the Dirac delta function here means that the distribution f is both spatially and temporally uncorrelated. One thing to mention is that, compared to conventional modal-analysis based approaches [38, 39] focusing on the long-term (i.e. when thermodynamic equilibrium is reached) average behavior of the system, transient response of the undulated membrane can also be captured here.

To implement this description in FEM simulation, a uniform load f_i^j was assumed to act on the area $A(\mathbf{x_i})$ (surrounding each node $\mathbf{x_i}$) over the time interval $[t_j t_{j+1}]$, that is

$$f_i^j = \frac{1}{A(\mathbf{x_i})(t_{j+1} - t_j)} \int_{A(\mathbf{x_i})} \int_{t_j}^{t_{j+1}} f(\mathbf{x_i}, t) dt dA \tag{19}$$

It can be shown that, according to Eq. (18), the so-called auto-correlation function of f_i^j takes the form

$$< f_i^j f_i^j >= \frac{2\mu k_B T}{A(\mathbf{x_i})\Delta t}, < f_i^j >= 0 \tag{20}$$

Essentially, the force acting on each nodal area must follow a Gaussian distribution with zero mean and a variance of $\frac{2\mu k_B T}{A(\mathbf{x_i})\Delta t}$. By adding this force to the expression of $\Delta\sigma$ in Eq. (8), we can then simulate the spontaneous shape fluctuations of the vesicle. For example, three snap-shots of a fluctuating vesicle are shown in Fig. 8.

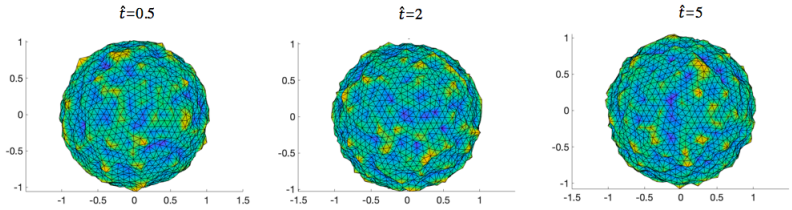

Figure 8: Snap-shots of an undulated vesicle (with zero in-plane tension). Here the normal displacement of membrane was amplified by 10 times for clear presentation.

It is noteworthy to point out that the shape undulation of quasi-spherical vesicles has been analyzed by several groups [40, 41, 42] before. For example,the fluctuating shape of a quasi-spherical vesicle can be represented as

$$R(\theta,\phi) = R_0(1 + \sum_{l\geq 0}^{l_{max}} \sum_{m=-l}^{l} u_{l,m} Y_{ml}(\theta,\phi)) \tag{21}$$

where θ and ϕ are two polar coordinates, R represents the radius and Y_{ml} is the so-called spherical harmonics function (with m and l being its order and degree respectively). From thermodynamic analysis, the long-term fluctuating amplitude associated with Y_{ml} can be found as [40]

$$< |u_{l,m}|^2 >= \frac{k_B T}{\kappa_b}[(l+2)(l-1)[(l+1)l+\Gamma]]^{-1}. \tag{22}$$

where Γ refers to vesicle tension restricting the fluctuation of membrane.

To compare our results with predictions from Eq.(22), we carried out simulations by setting $\kappa_b = 25 k_B T$ and $\rho = \rho_0$ (i.e. zero in-plane tension), and then monitored the radial position of membrane at an arbitrary point. As illustrated in Fig. 9(a), due to thermal excitations, the radial position fluctuated around the equilibrium value (i.e. the initial vesicle radius). Interestingly, after a short transition period, the average amplitude of such undulation, calculated by integration over the whole time period, began to converge to the value predicted by Eq. (22) with $\Gamma = 0$, refer to Fig. 9(b), which again demonstrates the validity and capability of our approach.

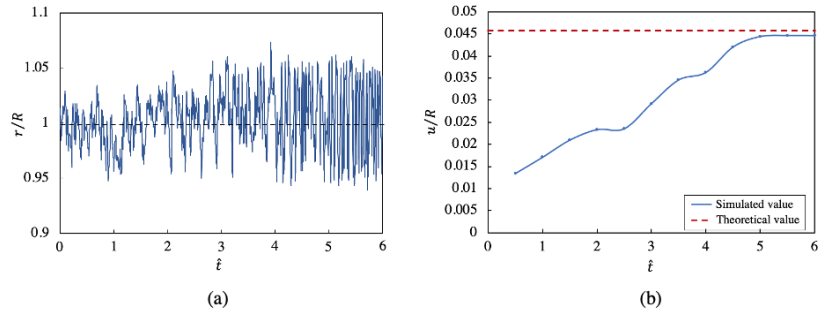

Figure 9: (a)Simulated radial position r (normalized by initial vesicle radius R) of membrane at an arbitrary point under zero in-plane tension. (b)Evolution of the normalized undulation amplitude (i.e. u/R) calculated from our simulations (solid line). Prediction from Eq.(22) is given by the dotted line where $l_{max} = 4$ was used as contributions from higher undulation modes were found to be negligible.

6 Conclusion

In this paper, we presented a novel computational framework to capture the combined fluid- and solid-like response of lipid membranes and then used it to investigate the enforced deformation and spontaneous shape fluctuation of lipid vesicles under a variety of experimental conditions. Specifically, we showed how transport of lipid molecules within the membrane modulates the in-plane tension distribution, as well as its coupling with the out-of-plane response of membrane. In addition, a self-consistent (Langevin dynamics based) method was also introduced (and then verified) to take into account spontaneous thermal undulations of membrane.

It must be pointed out that, compared to most existing FEM models, the diffusion of lipids and the viscous resistance of surrounding medium against the deformation of membrane are directly considered in the present formulation. Furthermore, the continuum nature of the model also allows us to carry out simulations on realistic spatial and temporal scales, something that could be difficult to achieve in molecular dynamics-based approaches [43, 44, 45]. In this regard, our model may serve as a computational platform for examining cellular processes such as the formation of polymerization-induced membrane protrusion/movement [46, 47], cell adhesion [48, 49] and migration [50, 51], where morphology change of the membrane and transport of lipids/transmembrane proteins are known to play key roles. In addition, the dynamic nature of our model also make it suitable for studying transient phenomena like endocytosis [52] and closed mitosis [53]. Investigations along these directions are underway.

7 Acknowledgement

This research was funded by the Research Grants Council of the Hong Kong Special Administration Region (Project No.: GRF/17257016, GRF/17210618), and the National Natural Science Foundation of China (Project No. 11872325).

References

[1] P. Singleton. Bacteria in Biology, Biotechnology and Medicine. *Wiley. pp.*, 5th ed.(ISBN 0- 471-98880-4):98880, 1999.

[2] Félix M. Goñi. The basic structure and dynamics of cell membranes: An update of the Singer-Nicolson model. *Biochimica et Biophysica Acta - Biomembranes*, 1838(6):1467–1476, 2014.

[3] Ronald A. Siegel. Random walks in biology. *Journal of Controlled Release*, 32(2):201–202, 1994.

[4] Nullin Divecha and Robin F Irvine. Phospholipid signaling. *Cell*, 80(2):269–278, jan 1995.

[5] Derek Marsh. Elastic curvature constants of lipid monolayers and bilayers. *Chemistry and Physics of Lipids*, 144(2):146–159, 2006.

[6] Hammad A Faizi, Shelli L Frey, and Rumiana Dimova. Bending rigidity of charged lipid bilayer membranes. *Soft Matter*, 15(29):6006–6013, Apr 2019.

[7] Jad Eid, Hefez Razmazmz, Alia Jraij, and Ali Ebrahimi. On calculating the bending modulus of lipid bilayer membranes from buckling simulations. *The Journal of Physical Chemistry B*, 124(29):6299–6311, Jul 2020.

[8] Italo V. Tasso and Gustavo C. Buscaglia. A finite element method for viscous membranes. *Computer Methods in Applied Mechanics and Engineering*, 255:226–237, 2013.

[9] Lin Ma and William S. Klug. Viscous regularization and r-adaptive remeshing for finite element analysis of lipid membrane mechanics. *Journal of Computational Physics*, 227(11):5816–5835, 2008.

[10] Roger A. Sauer, Thang X. Duong, Kranthi K. Mandadapu, and David J. Steigmann. A stabilized finite element formulation for liquid shells and its application to lipid bilayers. *Journal of Computational Physics*, 330:436–466, 2017.

[11] Feng Feng and William S. Klug. Finite element modeling of lipid bilayer membranes. *Journal of Computational Physics*, 220:394–408, dec 2006.

[12] S. J. Singer and G. L. Nicolson. The Fluid Mosaic Model of the Structure of Cell Membranes. *Sience*, 175:720–731, 1972.

[13] P. G. Saffman and M. Delbrueck. Brownian motion in biological membranes. *Proceedings of the National Academy of Sciences of the United States of America*, 72(8):3111–3113, 1975.

[14] P. G. Saffman. Brownian motion in thin sheets of viscous fluid. *Journal of Fluid Mechanics*, 73(4):593–602, 1976.

[15] Emmanuel Boucrot, Adi Pick, Gamze Çamdere, Nicole Liska, Emma Evergren, Harvey T. McMahon, and Michael M. Kozlov. Membrane fission is promoted by insertion of amphipathic helices and is restricted by crescent BAR domains. *Cell*, 149(1):124–136, 2012.

[16] Z.T Graber, T Shi, and T Baumgart. Cations induce shape remodeling of negatively charged phospholipid membranes. *Physical Chemistry Chemical Physics*, 19(23):15285–15295, 2017.

[17] Ana-Nicoleta Bondar and Sandro Keller. Lipid membranes and reactions at lipid interfaces: Theory, experiments, and applications. *The Journal of Membrane Biology*, 251(3):295–298, 2018.

[18] Jakob Andersson, A Fuller, and Kathleen Wood. A tethered bilayer lipid membrane that mimics microbial membranes. *Physical Chemistry Chemical Physics*, 20(18):12958–12969, 2018.

[19] Daniel Balleza. Mechanical properties of lipid bilayers and regulation of mechanosensitive function. *Channels*, 6(4):220–233, 2012.

[20] Amelie Bacle, Romain Gautier, Catherine.L Jackson, and Stefano Vanni. Interdigitation between triglycerides and lipids modulates surface properties of lipid droplets. *Biophysical Journal*, 112(7):1417–1430, 2017.

[21] David Boal. *Mechanics of the Cell*. Cambridge University Press, 2 edition, 2012.

[22] Kinneret Keren, Zachary Pincus, Greg M. Allen, Erin L. Barnhart, Gerard Marriott, Alex Mogilner, and Julie A. Theriot. Mechanism of shape determination in motile cells. *Nature*, 453(7194):475–480, May 2008.

[23] W. Helfrich and R. M. Servuss. Undulations, steric interaction and cohesion of fluid membranes. *Il Nuovo Cimento D*, 3(1):137–151, 1984.

[24] W. Janke and H. Kleinert. Fluctuation pressure of membrane between walls. *Physics Letters A*, 117(7):353–357, 1986.

[25] P. R. Zarda, S. Chien, and R. Skalak. Elastic deformations of red blood cells. *Journal of Biomechanics*, 10(4):211–221, 1977.

[26] Chao Fang, Fan Zheng, Jiaxing Yao, Xi Wei, Chuanhai Fu, Xinghua Shi and Yuan Lin. A Model for Bridging Microtubule Dynamics with Nuclear Envelope Shape Evolution during Closed Mitosis. *Journal of the Mechanics and Physics of Solids (In press)*.

[27] Chao Fang, T. H. Hui, X. Wei, X. Shao, and Yuan Lin. A combined experimental and theoretical investigation on cellular blebbing. *Scientific Reports*, 7(1), 2017.

[28] C. Pozrikidis. Boundary Integral and Singularity Methods for Linearized Viscous Flow. *Boundary Integral and Singularity Methods for Linearized Viscous Flow*, 1992.

[29] Conglin Lu, Yan Cao, and David Mumford. Surface evolution under curvature flows. *Journal of Visual Communication and Image Representation*, 13(1-2):65–81, 2002.

[30] Mathieu Desbrun, Mark Meyer, Peter Schröder, and Alan H. Barr. Implicit fairing of irregular meshes using diffusion and curvature flow. *Proceedings of the 26th Annual Conference on Computer Graphics and Interactive Techniques, SIGGRAPH 1999*, pages 317–324, 1999.

[31] Denis Wirtz. Particle-tracking microrheology of living cells: Principles and applications. *Annual Review of Biophysics*, 38(1):301–326, 2009.

[32] P. R. Zarda, S. Chien, and R. Skalak. Elastic deformations of red blood cells. *Journal of Biomechanics*, 10(4):211–221, 1977.

[33] Reinhard Lipowsky. The conformation of membranes. *Nature*, 349(6309):475–481, 1991.

[34] W. Helfrich and R. M. Servuss. Undulations, steric interaction and cohesion of fluid membranes. *Il Nuovo Cimento D*, 3(1):137–151, 1984.

[35] H. Kleinert. Fluctuation pressure of membrane between walls. *Physics Letters, Section A: General, Atomic and Solid State Physics*, 257(5-6):269–274, 1999.

[36] Bin Hu, V. B. Shenoy, and Yuan Lin. Buckling and enforced stretching of bio-filaments. *Journal of the Mechanics and Physics of Solids*, 60(11):1941–1951, 2012.

[37] Yuan Lin, X. Wei, J. Qian, K. Y. Sze, and V. B. Shenoy. A combined finite element-Langevin dynamics (FEM-LD) approach for analyzing the mechanical response of bio-polymer networks. *Journal of the Mechanics and Physics of Solids*, 62(1):2–18, 2014.

[38] Long Li, Xiaohuan Wang, Yingfeng Shao, Wei Li, and Fan Song. Entropic pressure between fluctuating membranes in multilayer systems. *Science China: Physics, Mechanics and Astronomy*, 61(12), 2018.

[39] Long Li and Fan Song. Entropic force between biomembranes. *Acta Mechanica Sinica/Lixue Xuebao*, 32(5):970–975, 2016.

[40] Xavier Michalet, David Bensimon, and Bertrand Fourcade. Fluctuating vesicles of nonspherical topology. *Physical Review Letters*, 72(1):168–171, 1994.

[41] David C. Morse and Scott T. Milner. Statistical mechanics of closed fluid membranes. *Physical Review E*, 52(6):5918–5945, 1995.

[42] Eric R. May, Atul Narang, and Dmitry I. Kopelevich. Role of molecular tilt in thermal fluctuations of lipid membranes. *Physical Review E - Statistical, Nonlinear, and Soft Matter Physics*, 76(2), 2007.

[43] Xin Yi and Huajian Gao. Cell interaction with graphene microsheets: Near-orthogonal cutting versus parallel attachment. *Nanoscale*, 7(12):5457–5467, 2015.

[44] Miaorong Yu, Lu Xu, Falin Tian, Qian Su, Nan Zheng, Yiwei Yang, Aohua Wang, Chunliu Zhu, Shiyan Guo, Xinxin Zhang, Yong Gao, Xinghua Shi, and Huajian Gao. Rapid transport of deformation-tuned nanoparticles across biological hydrogels and cellular barriers. *Nature Communications*, 9(1):2607, 2018.

[45] Yanbing Yang, Xiangdong Yang, Ling Liang, Huanyu Cheng, Renzhi Ma, Quan Yuan, and Xiangfeng Duan. Large-area graphene-nanomesh/carbon-nanotube hybrid membranes for ionic and molecular nanofiltration. *Science*, 364(6445):1057–1062, 2019.

[46] Yuan Lin. Mechanics model for actin-based motility. *Physical Review E - Statistical, Nonlinear, and Soft Matter Physics*, 79(2), 2009.

[47] Lei Yang, Ze Gong, Yuan Lin, Viswanath Chinthapenta, Qunyang Li, Thomas J. Webster, and Brian W. Sheldon. Disordered Topography Mediates Filopodial Extension and Morphology of Cells on Stiff Materials. *Advanced Functional Materials*, 27(38), 2017.

[48] Long Li, Jinglei Hu, Guangkui Xu, and Fan Song. Binding constant of cell adhesion receptors and substrate-immobilized ligands depends on the distribution of ligands. *Physical Review E*, 97(1), 2018.

[49] Guang Kui Xu, Xi Qiao Feng, Hong Ping Zhao, and Bo Li. Theoretical study of the competition between cell-cell and cell-matrix adhesions. *Physical Review E - Statistical, Nonlinear, and Soft Matter Physics*, 80(1), 2009.

[50] Yuan Lin, V. B. Shenoy, Bin Hu, and Limiao Bai. A microscopic formulation for the actin-driven motion of Listeria in curved paths. *Biophysical Journal*, 99(4):1043–1052, 2010.

[51] Yuan Lin. A model of cell motility leading to biphasic dependence of transport speed on adhesive strength. *Journal of the Mechanics and Physics of Solids*, 58(4):502–514, 2010.

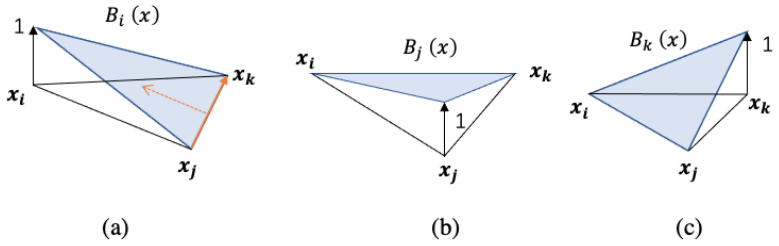

Figure A1: Areal interpolation functions adopted for the triangle element.

[52] Yi Xin, Shi Xinghua, and Gao Huajian. Cellular uptake of elastic nanoparticles. *Physical Review Letters*, 107(9):98101, 2011.

[53] Qian Zhu, Fan Zheng, Allen P. Liu, Jin Qian, Chuanhai Fu, and Yuan Lin. Shape Transformation of the Nuclear Envelope during Closed Mitosis. *Biophysical Journal*, 111(10):2309–2316, 2016.

[54] Mark Meyer, Mathieu Desbrun, Peter Schröder, and Alan H. Barr. Discrete Differential-Geometry Operators for Triangulated 2-Manifolds. pages 35–57, 2003.

A Appendix - Details of FEM implementation

As illustrated in Fig. 2, the domain $A(\mathbf{x_i})$ of nodal point $\mathbf{x_i}$ (within the triangular mesh) can be defined as the one with each side of its boundary $\partial A(\mathbf{x_i})$ crossing the mid-point of the segment $\mathbf{x_i x_j}$ that connects $\mathbf{x_i}$ with a neighboring nodal point $\mathbf{x_j}$. Two opposite angles α_{ij} and β_{ij}, with respect to $\mathbf{x_i x_j}$, can then be defined accordingly, refer to Fig. 2.

Within each triangle element, the conventional areal shape functions B_1, B_2 and B_3 (see Fig. A1) were used to interpolate different variables. Under such circumstance, the gradient of a piece-wise linear function$f$ (within the mesh) can be calculated as

$$\begin{aligned} \nabla f(\mathbf{u}) &= f_i \nabla B_i(\mathbf{u}) + f_j \nabla B_j(\mathbf{u}) + f_k \nabla B_k(\mathbf{u}) \\ &= (f_j - f_i)\nabla B_j(\mathbf{u}) + (f_k - f_i) B_k(\mathbf{u}) \end{aligned} \tag{A1}$$

where $\mathbf{u}$ represents any point within the triangle element, $f_i = f(\mathbf{x_i})$, $f_j = f(\mathbf{x_j})$ and $f_k = f(\mathbf{x_k})$. Note that, the gradient of the shape function takes the form

$$\nabla B_i(\mathbf{u}) = \frac{(\mathbf{x_k} - \mathbf{x_j})^{\perp}}{2A_t} \tag{A2}$$

where the symbol $\perp$ means a counterclockwise rotation of 90 degrees as show in Fig. A1(a). Divergence theorem implies that

$$\begin{aligned}\int_A \Delta f(\mathbf{u}) dA &= \int_A div \nabla f(\mathbf{u}) dA \\ &= \int_{\partial A} \nabla f(\mathbf{u}) \cdot \mathbf{n}(\mathbf{u}) dS\end{aligned} \tag{A3}$$

where $\mathbf{n}$ is the outward normal vector of boundary ∂A, eventually leading to

$$\begin{aligned}\int_{\partial A} \nabla f(\mathbf{u}) \cdot \mathbf{n}(\mathbf{u}) dS &= \frac{1}{2} \nabla f(\mathbf{u}) (\mathbf{x_j} - \mathbf{x_k})^{\perp} \\ &= (f_j - f_i) \frac{(\mathbf{x_i} - \mathbf{x_k})^{\perp} (\mathbf{x_j} - \mathbf{x_k})^{\perp}}{4A_t} \\ &\quad + (f_k - f_i) \frac{(\mathbf{x}_j - \mathbf{x}_i)^{\perp} (\mathbf{x}_j - \mathbf{x}_k)^{\perp}}{4A_t}\end{aligned} \tag{A4}$$

Finally, the so-called average Laplace-Beltrami (over a certain region) can be expressed as [54]

$$\int_A \Delta f(\mathbf{u}) dA = \frac{\sum_{\mathbf{u_j} \in N_1(\mathbf{u_i})} (\cot \alpha_{ij} + \cot \beta_{ij})(f_j - f_i)}{2} \tag{A5}$$

$$\Delta f(\mathbf{u_i}) = \frac{\sum_{\mathbf{u_j} \in N_1(\mathbf{u_i})} (\cot \alpha_{ij} + \cot \beta_{ij})(f(\mathbf{x_j}) - f(\mathbf{x_i}))}{2A(\mathbf{x_i})} \tag{A6}$$

where $\mathbf{x_j}$ is the set of the neighboring vertices around $\mathbf{x_i}$ (Fig. 2) while α_{ij} and β_{ij} are the two opposite angles of edge $\mathbf{x_i x_j}$.